

Jadwiga Zalewska, Jan Kaczmarczyk
Oil and Gas Institute, Kraków

Analysis of rock samples' internal pore structure based on X-ray computed microtomography data. Part I

Introduction

The aim of the study was evaluation of Upper Rotliegend sandstone samples pore space, originating from G-1, O-3 and R-1, 2, 3 boreholes where natural gas or natural gas and brine were extracted. Analysed profiles of Upper Rotliegend are dominated by Aeolian sandstones. Only Aeolian dune facies and secondary interdune Aeolian fa-

cies sandstones are present in profiles of boreholes R-1, 2 and 3. Lacustrine sediments, representing marginal playa, sandy playa and sporadically clay playa facies are present in the Upper Rotliegend roof in the rest of the profiles. Fluvial deposit interbeddings appear in the bottom parts of boreholes G-1 and O-3.

Examination results

The examinations were carried out with Benchtop CT-160X X-ray microtomograph according to detailed methodology described in detail in Dohnalik et al. [1],

Zalewska et al. [2009]. The principle of the examination with the use of computed microtomography method is outlined in the fig. 1.

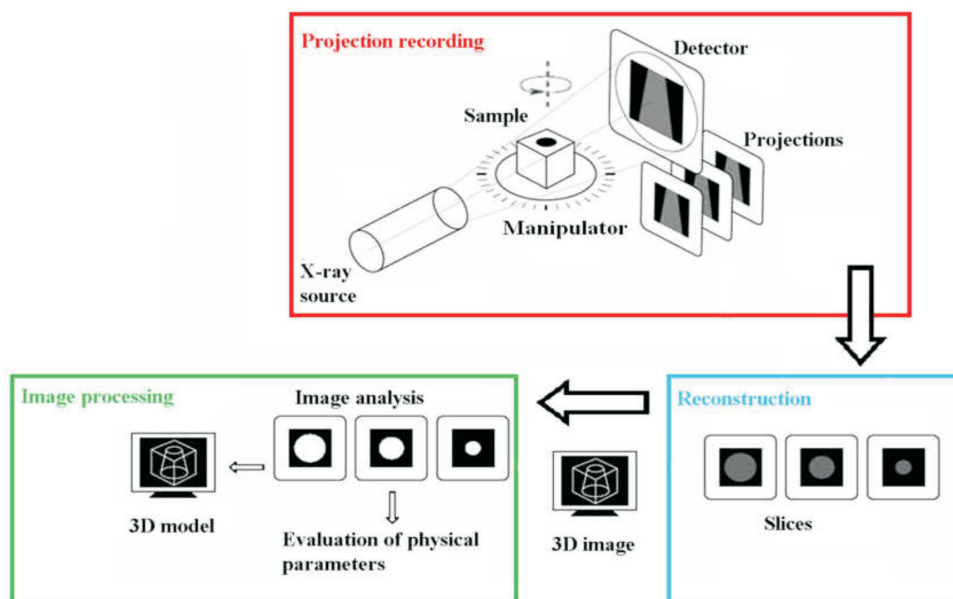


Fig. 1. Computed X-ray microtomography operating principle

The results obtained with the use of computer X-ray microtomography enabled interpretation of pore network structure for examined samples. For the purposes of simplification of obtained results analysis, the pores were grouped in three sets:

- small pores: $2 \times 10^2 \div 2 \times 10^5 \mu\text{m}^3$ (I÷III volume class),
- medium pores: $2 \times 10^5 \div 2 \times 10^7 \mu\text{m}^3$ (IV÷V volume class),
- large pores: above $2 \times 10^7 \mu\text{m}^3$ (VI volume class).

12 samples from G-1 borehole were examined, which led to the finding that four of them had well developed internal pore network (10730, 10729, 10727, 10726), three samples had very weakly developed pore structure, and five of them had been classified as having weakly developed pore structure. The samples of well developed internal pore network are characterized with low fraction

of I, II, and III volume class (tab. 1, fig. 2 & 3). VI volume class that often dominates in pore space of sample, is present in all of the samples. 3D visualizations reveal distinct non-uniformity of porosity distribution, and also areas of lowered porosity may be noted (for example, 10726, fig. 2 & 3), probably connected with sedimentation structures. The pores are distributed in non-uniform manner which is proved by high porosity difference between individual subsamples (for example 10726A and 10726B). All samples from this group represented Aeolian dune sandstones of A2 facies. The sample 10729 from this well features best developed pore structure where one pore belonging to VI Class in both subsamples constitutes over 80% of the whole pore space volume. The remaining 20% is approximately equally divided between pores belonging to lower classes (fig. 2 & 3).

Table 1. List of individual pore volume classes fraction for samples from G-1 borehole

Sample No.	Facies	Class Fraction [%]					
		Subsample A			Subsample B		
		I÷III	IV÷V	VI	I÷III	IV÷V	VI
10734	P2	0.0	0.0	0.0	97.6	2.4	0.0
10733	P2	0.0	0.0	0.0	0.0	0.0	0.0
10732	A2	60.8	39.2	0.0	67.7	32.2	0.0
10731	A2	70.2	29.9	0.0	49.8	50.2	0.0
10730	A2	19.6	47.4	32.8	26.7	53.4	19.9
10729	A2	10.1	8.5	81.5	10.1	7.2	82.6
10728	A4	59.1	33.1	7.8	59.9	40.1	0.0
10727	A2	42.6	48.1	9.2	44.2	50.4	5.4
10726	A2	9.4	21.7	68.9	5.0	7.1	87.9
10725	A2	83.4	16.6	0.0	41.8	58.2	0.0
10724	A2	57.2	34.0	8.8	75.3	24.6	0.0
10723	A4	94.4	5.50	0.0	97.4	2.6	0.0

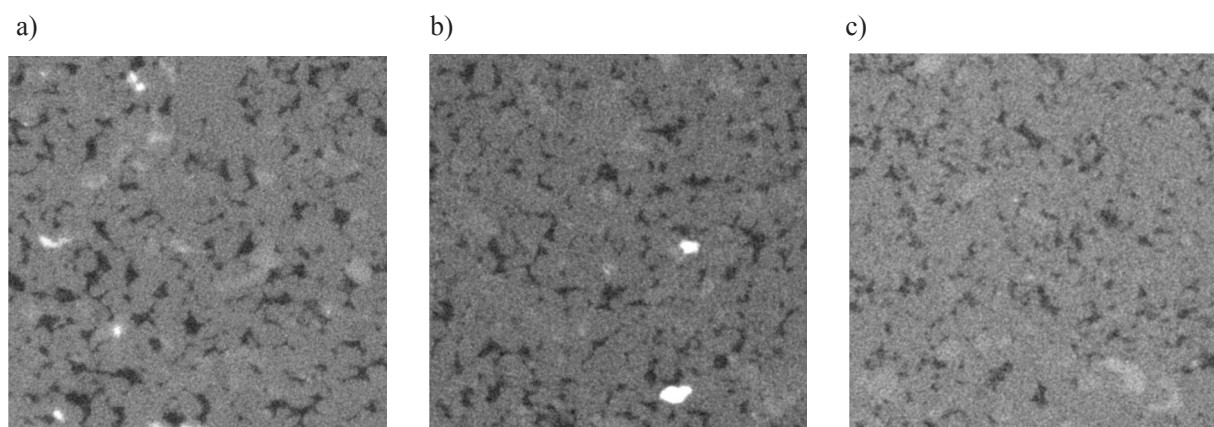


Fig. 2. Sections of samples from G-1 borehole with well developed pore structure

a) 10726A sample, b) 10729A sample, c) 10730A sample

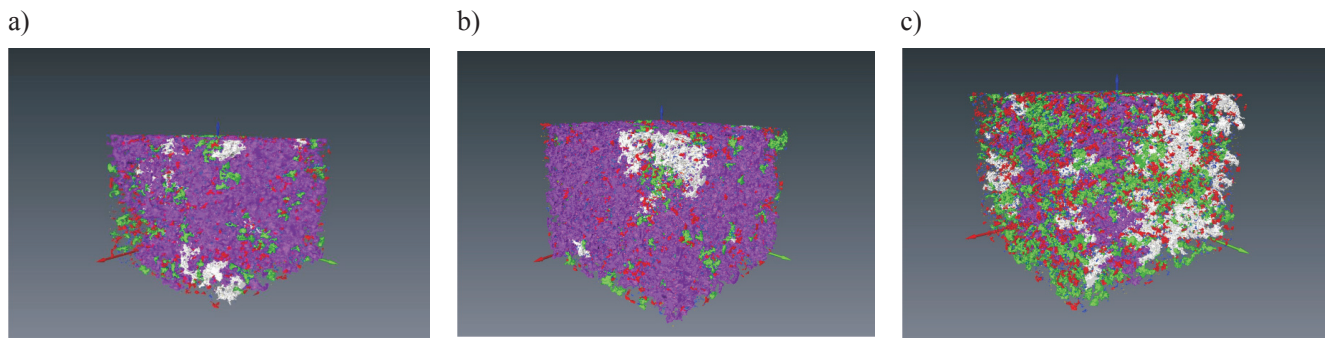


Fig. 3. 3D visualization of well developed pore structure for samples from borehole G-1

a) 10726A sample, b) 10729A sample, c) 10730A sample

The sections of samples with well developed pore structure, shown in fig. 2, were presented in form of 3D visualization in fig. 3.

Five samples from borehole G-1 were classified as possessing weakly developed pore structure, featuring non-uniform distribution of small and medium volume pores. The VI Class was missing in these samples, with dominating fraction of IV and V Classes or comparable fraction of both IV÷V and I÷III volume classes (tab. 1,

fig. 4 & 5). Only one sample (10728) was representative of Aeolian dune sandstones of A4 facies, while the remaining originated from A2 facies.

The 10734 and 10733 samples, representing P2 facies playa unit, and 10723 sample of A4 facies Aeolian sandstone were considered samples of weakly developed internal pore network. Examinations of 10733 sample pore structure, carried out at 5.8 μm image resolution revealed no pores in any of the directions under analysis.

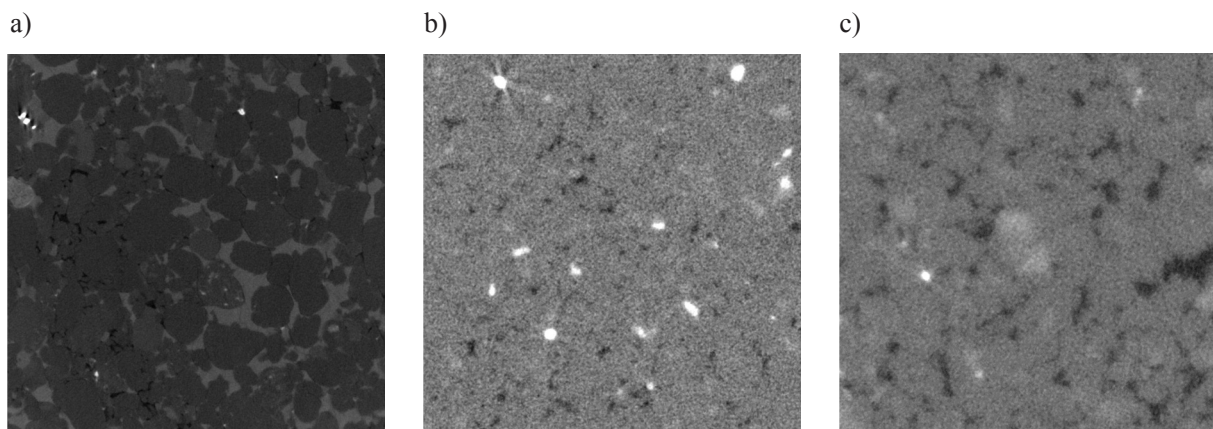


Fig. 4. Sections of samples from borehole G-1 with weakly developed pore structure

a) 10731B sample, b) 10728B sample, c) 10725B sample

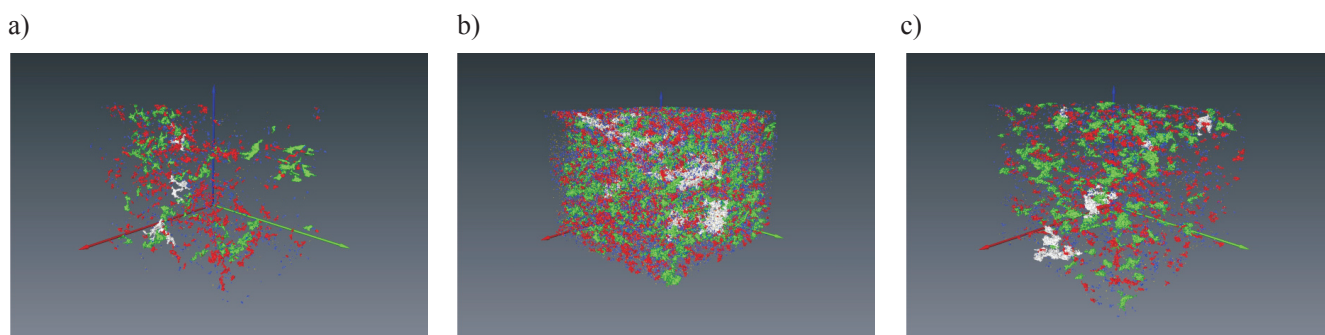


Fig. 5. 3D pore space visualization of samples with weakly developed pore structure (borehole G-1)

a) 10731B sample, b) 10728B sample, c) 10725B sample

The remaining samples from this group featured lack of VI Class, small fraction of IV and V Classes, and high fraction of I-III classes of pore volumes (tab. 1, fig. 6 & 7).

12 samples from borehole O-3 were examined, six of which featured well developed internal pore network, four of them – weakly, and two of them very weakly developed pore structure (tab. 2).

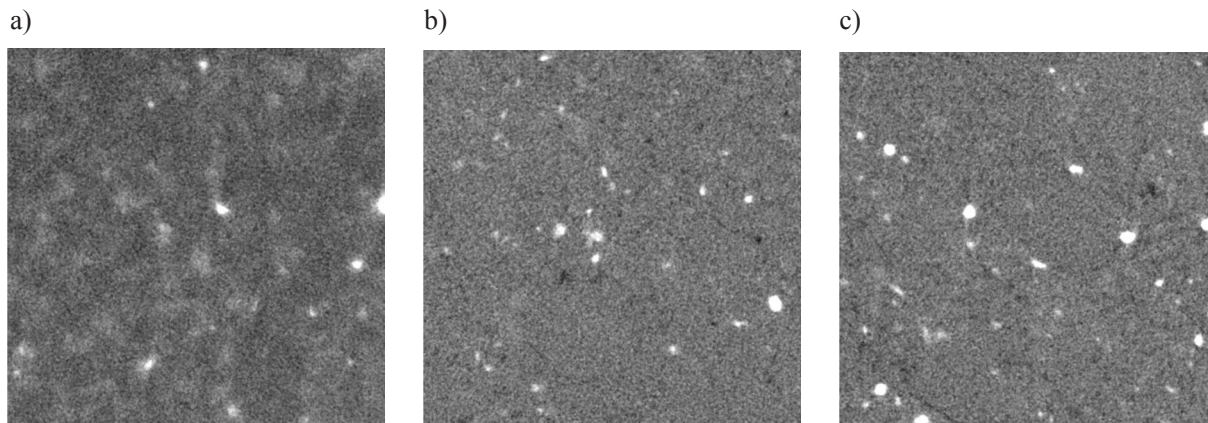


Fig. 6. Sections of samples (borehole G-1) with weakly developed pore structure

a) 10734B sample, b) 10723A sample, c) 10723B sample

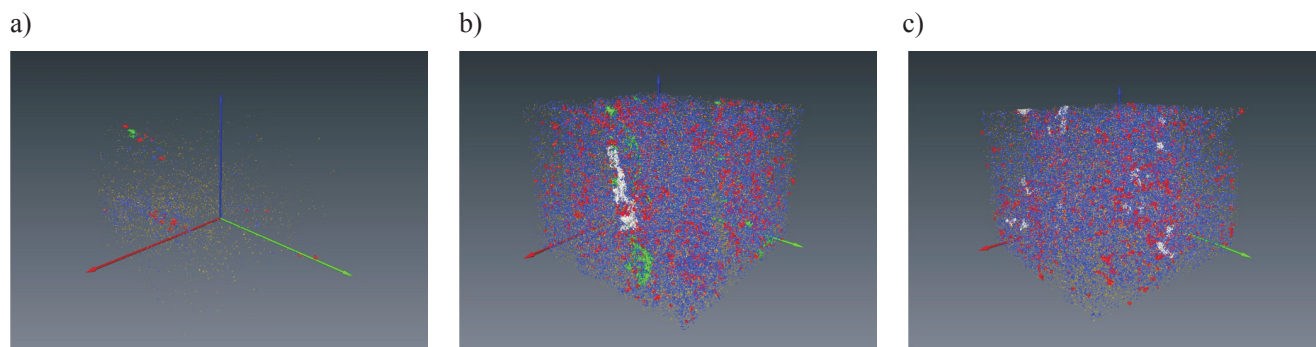


Fig. 7. 3D pore structure visualization for samples with weakly developed pore structure (borehole G-1)

a) 10734B sample, b) 10723A sample, c) 10723B sample

Table 2. List of individual pore volume classes fractions for samples from borehole O-3

Sample No.	Facies	Percentage of class fraction [%]					
		Subsample A			Subsample B		
		I÷III	IV÷V	VI	I÷III	IV÷V	VI
10746	P2	100.0	0.0	0.0	100.0	0.0	0.0
10745	P1	92.4	7.6	0.0	88.4	11.6	0.0
10744	A2	65.1	34.9	0.0	62.9	37.1	0.0
10743	A2	10.9	1.5	87.7	13.0	1.9	84.4
10742	A5	76.4	23.6	0.0	80.3	19.7	0.0
10741	A4	70.2	29.8	0.0	88.7	11.3	0.0
10740	A2	34.2	47.0	18.8	36.8	42.5	20.7
10739	A2	21.8	44.2	34.0	24.1	55.8	20.1
10738	A2	83.3	16.7	0.0	82.2	17.8	0.0
10737	A2	11.6	3.4	85.0	14.2	8.7	77.0
10736	A2	22.4	15.1	62.5	31.3	20.3	48.3
10735	A2	65.4	23.0	11.6	54.6	26.6	18.7

Samples of well developed pore structure (10743, 10740, 10739, 10737, 10736, 10735) were those that had large pores of dimensions exceeding $2 \times 10^7 \mu\text{m}^3$, constituting the VI volume class (tab. 2, fig. 8 & 9). Fraction of pores belonging to lower volume classes (I-V) is rather low and uniformly distributed. Two samples, 10743 and 10737, are distinguished with best developed pore structure, in which VI volume class occupies 88% and 84% respectively and constitutes a single object. All samples in this group are Aeolian dune sandstones from A2 facies.

Samples possessing weakly developed pore structure are Aeolian dune sandstones of various facies (A2, A4 & A5). They feature non-uniform layout of pores having small ($2 \times 10^2 \div 2 \times 10^5 \mu\text{m}^3$) and medium ($2 \times 10^5 \div 2 \times 10^7 \mu\text{m}^3$) volumes, and the lack of high volume pores (above $2 \times 10^7 \mu\text{m}^3$) (tab. 2, fig. 10 & 11). I-V volume classes were present, while fraction of V class being usually low, and modal value corresponded to II or III volume class (tab. 2, fig. 10 & 11).

Samples of weakly developed pore structure (borehole O-3) originated from P2 sand playa and P1 marginal playa facies. They were characterized by the presence of

small pores ($2 \times 10^2 \div 2 \times 10^5 \mu\text{m}^3$) and represented I-III volume classes (tab. 2, fig. 12 & 13). The fraction of class V and VI was null.

13 samples were examined from R region, covering three boreholes (R-1, 2, 3). One sample of good parameters, and four samples of weak parameters were found for R-1 borehole. In boreholes R-2 and R-3, two samples with good parameters, one sample with weak parameters and one sample with bad pore space parameters were found (tab. 3). Apart from 10755 and 10756 samples, originating from A2/A5 facies, all the remaining samples belonged to A2 facies.

Samples featuring well developed pore structure (10753, 10754, 10757, 10760 and 10761) are Aeolian dune sandstones from A2 facies, which contained pores belonging to VI class and volume exceeding $2 \times 10^7 \mu\text{m}^3$. The fraction of pores belonging to lower classes (10761 sample being an exception) constitutes over 50% of pore structure volume (tab. 3, fig. 14 & 15). The best developed structure of pore network can be seen in samples 10753 and 10761.

Samples with weakly developed pore structure (A2-10749, 10750, 10751, 10752 and 10759 facies, A2/A5 10755 facies) had pores belonging to I-V classes. They fea-

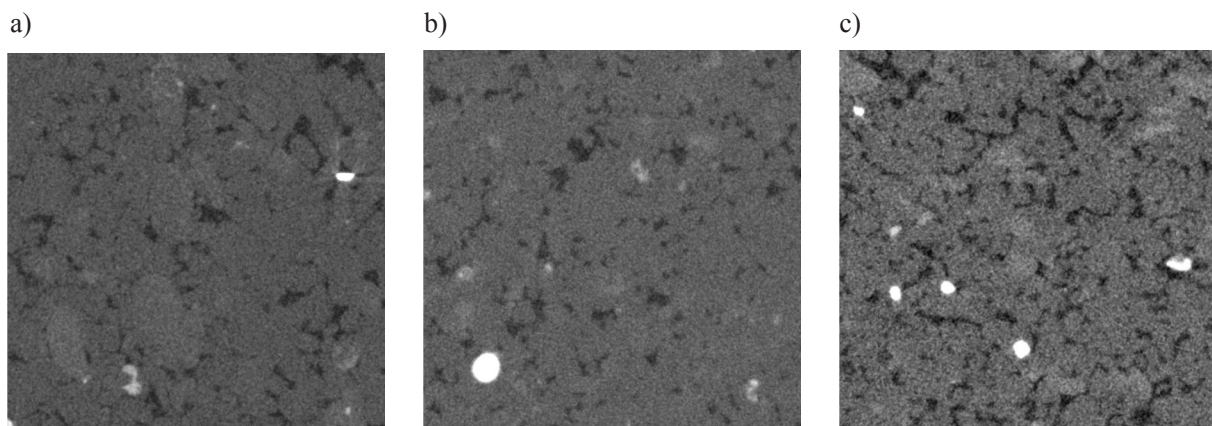


Fig. 8. Sections of samples from borehole O-3 with well developed pore structure

a) 10736A sample, b) 10740A sample, c) 10743A sample

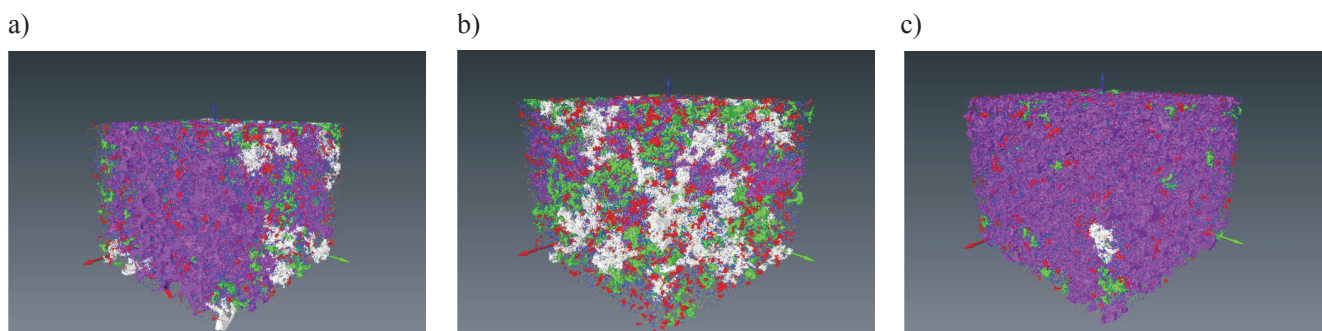


Fig. 9. 3D pore structure visualization for samples from borehole O-3 with well developed pore structure

a) 10736A sample, b) 10740A sample, c) 10743A sample

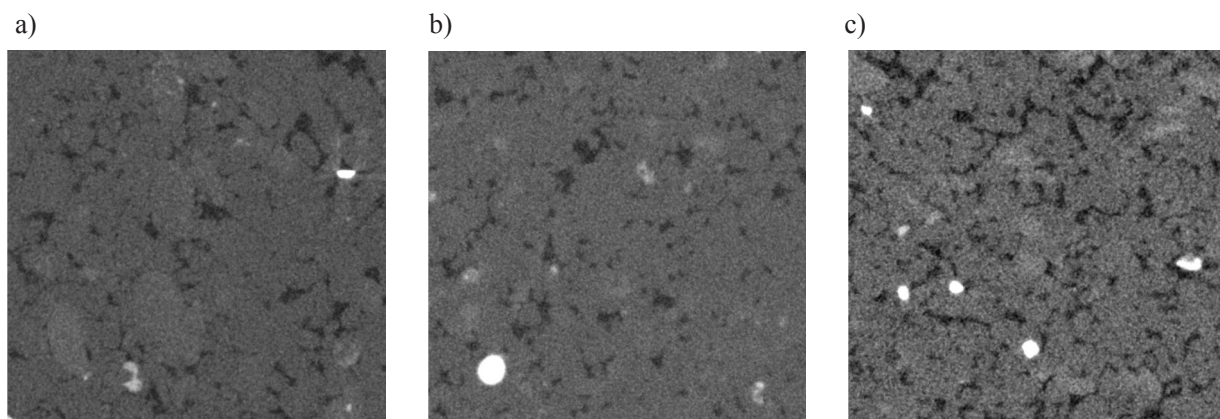


Fig. 10. Sections of samples from borehole O-3 with weakly developed pore structure
 a) 10744A sample, b) 10742A sample, c) 10741B sample

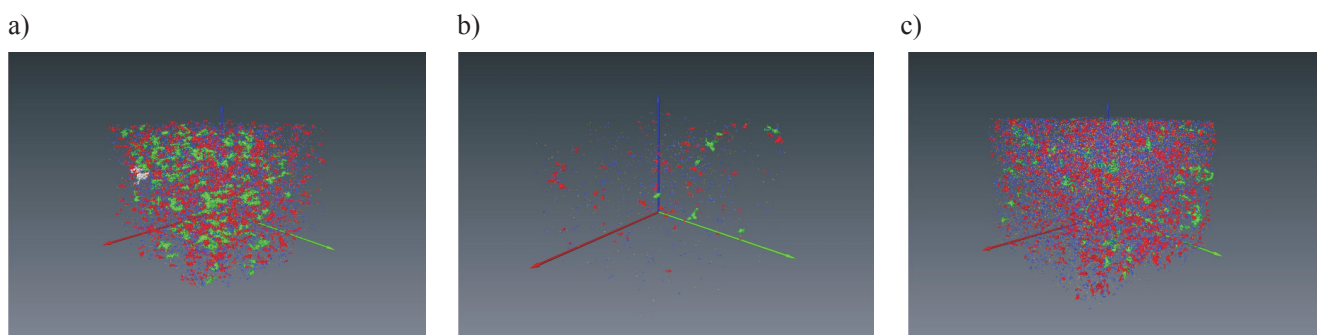


Fig. 11. 3D pore structure visualization for samples with weakly developed pore structure (borehole O-3)
 a) 10744A sample, b) 10742A sample, c) 10741B sample

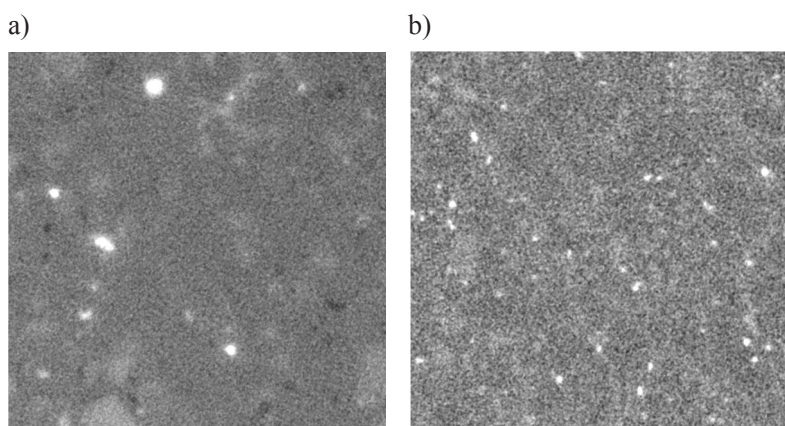
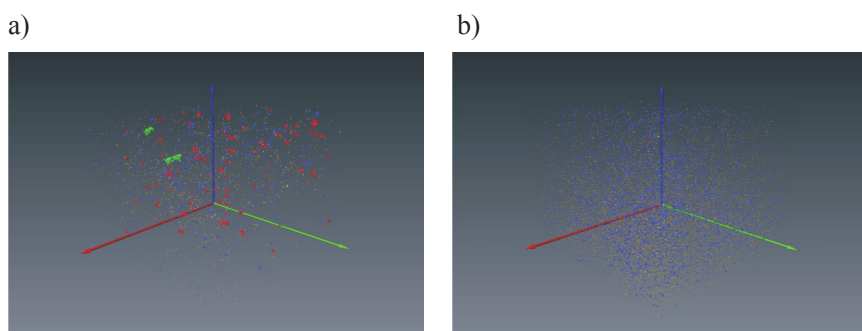


Fig. 12. Sections of samples from borehole O-3 with weakly developed pore structure
 a) 10745A sample, b) 10746A sample



Rys. 13. 3D pore structure visualization for samples with weakly developed pore structure (borehole O-3)
 a) 10745A sample, b) 10746A sample

Table 3. List of individual classes of pore volume percentage for R region samples

Sample No.	Facies	Percentage of class fraction [%]					
		Subsample A			Subsample B		
		I-III	IV-V	VI	I-III	IV-V	VI
10749	A2	60.5	39.5	0.0	64.3	35.8	0.0
10750	A2	35.7	64.3	0.0	33.0	67.0	0.0
10751	A2	72.6	27.5	0.0	67.9	32.1	0.0
10752	A2	65.7	34.3	0.0	53.9	46.0	0.0
10753	A2	23.6	44.6	31.7	20.0	33.2	46.8
10754	A2	38.4	53.2	8.4	33.2	48.4	18.4
10755	A2/A5	22.2	8.1	69.7	83.0	17.1	0.0
10756	A2/A5	91.1	9.0	0.0	90.4	9.7	0.0
10757	A2	45.9	41.7	12.4	28.2	34.4	37.4
10758	A2	96.7	3.3	0.0	96.2	3.8	0.0
10759	A2	77.9	22.1	0.0	71.3	28.6	0.0
10760	A2	45.5	34.1	20.3	56.1	28.0	15.8
10761	A2	9.0	14.4	76.5	9.4	13.5	77.1

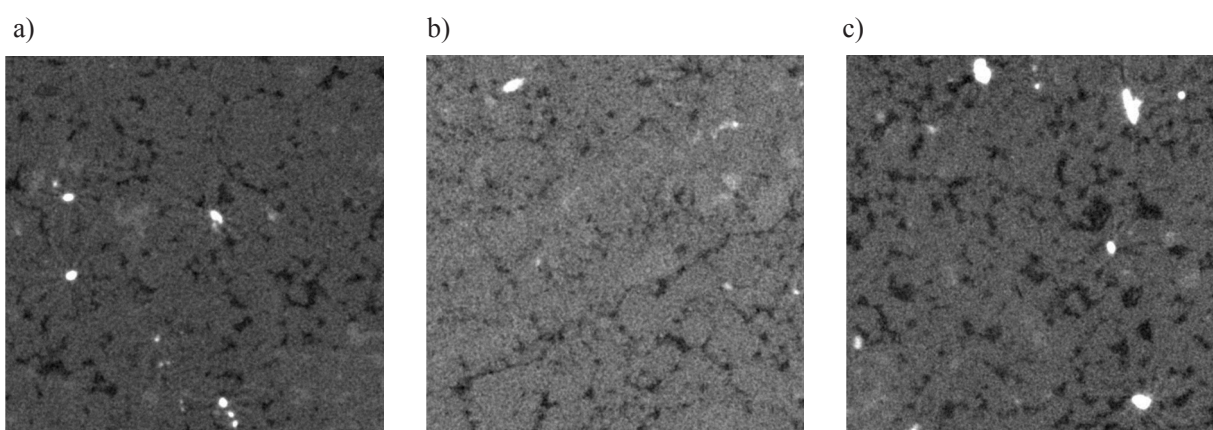


Fig. 14. Sections of samples from R region with well developed pore structure

a) 10753B sample, b) 10757B sample, c) 10761B sample

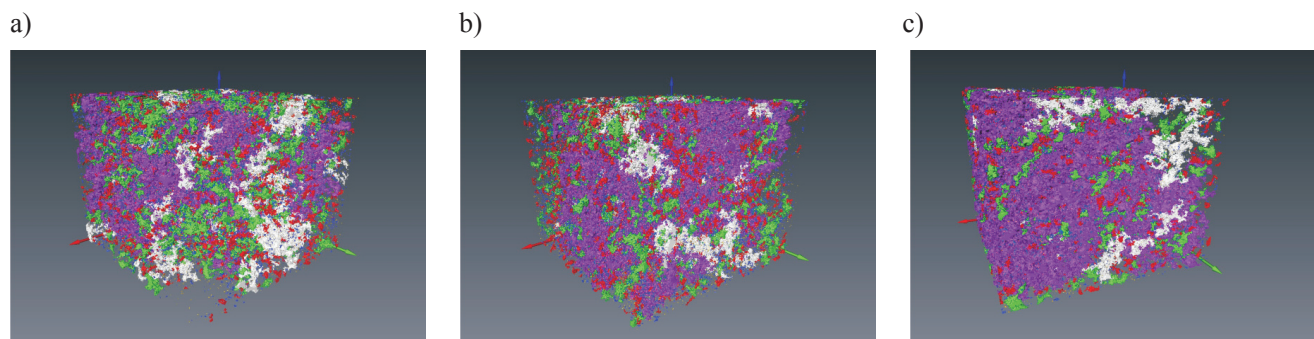


Fig. 15. 3D pore structure visualization for samples with well developed pore structure from R region

a) 10753B sample, b) 10757B sample, c) 10761B sample

tured high fraction of I÷III classes ($2 \times 10^2 \div 2 \times 10^5 \mu\text{m}^3$), above 55% in average (tab. 3, fig. 16 & 17). Apart from two

samples (10752, 10755), the remaining ones are characterized by uniform distribution of pore classes.

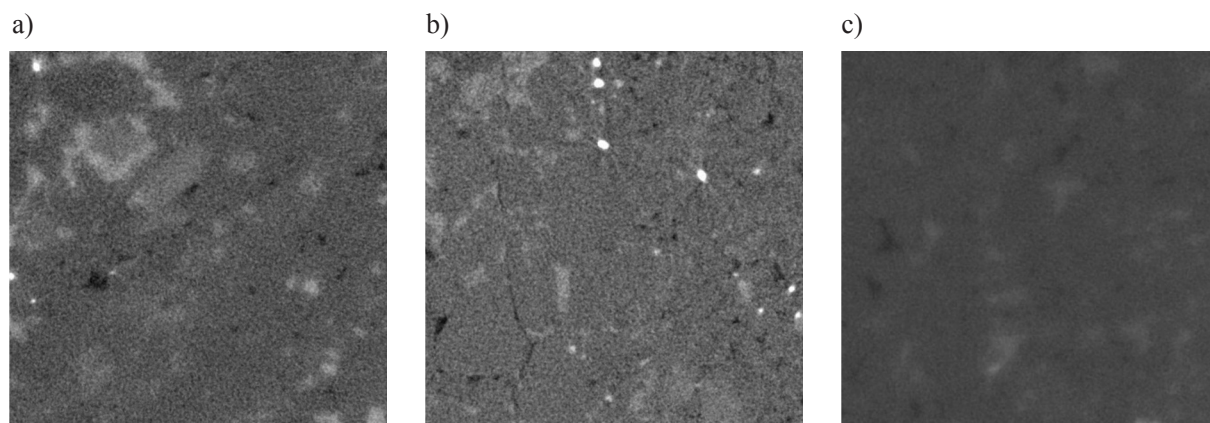


Fig. 16. Sections of samples from R region with weakly developed pore structure
 a) 10749A sample, b) 10751B sample, c) 10759A sample

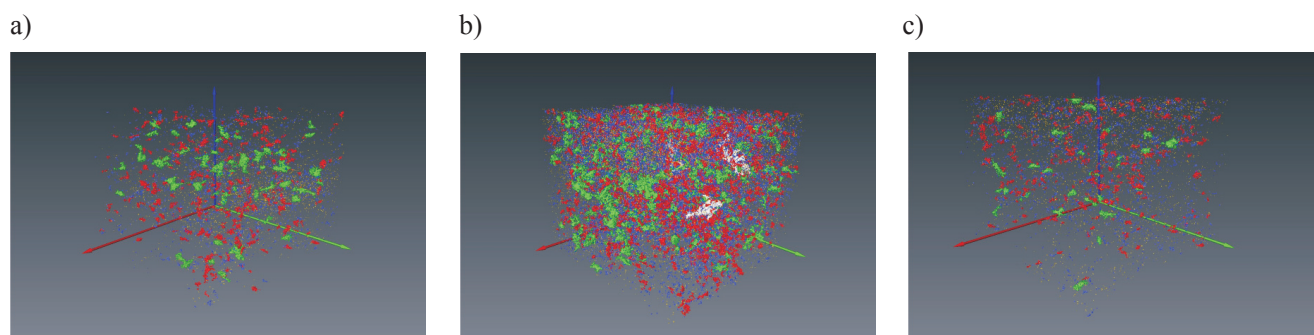


Fig. 17. 3D pore structure visualization for samples with weakly developed pore structure from R region
 a) 10749A sample, b) 10751B sample, c) 10759A sample

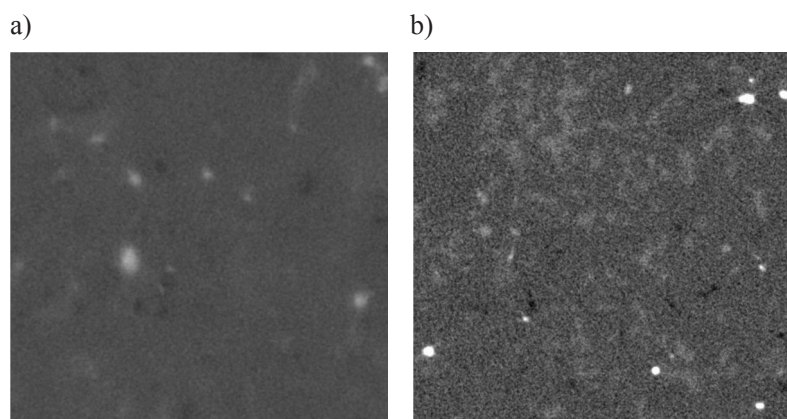


Fig. 18. Sections of samples from R region with weakly developed pore structure
 a) 10756B sample, b) 10758B sample

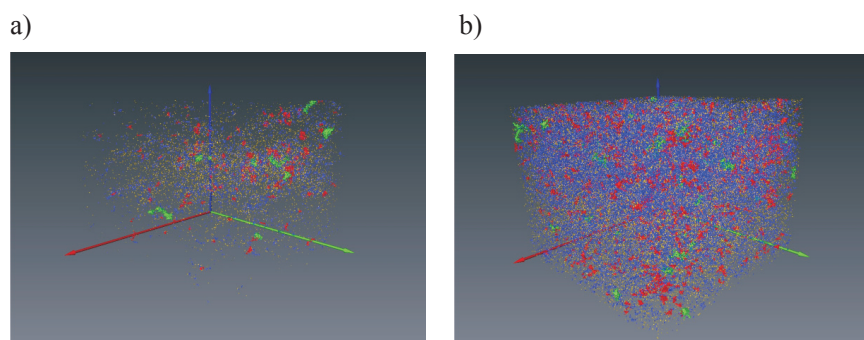


Fig. 19. 3D pore structure visualization for samples with weakly developed pore structure from R region
 a) 10756B sample, b) 10758B sample

Samples with weakly developed pore structure (10756, 10758) featured very high fraction of low volume pores $2 \times 10^2 \div 2 \times 10^5 \mu\text{m}^3$ (over 90%) (tab. 3, fig. 18 & 19) corresponding to I-III classes; objects from IV-V classes occurred in the remaining, minor part of pore structure.

Next, the results of porous channels geometric tortuosity (τ) obtained from micro-CT data (details found in Zalewska et al., 2009) were analysed. This parameter was analysed for all samples, but computed only in cases when connections of pore channels between two opposite sides of subsample were present in the direction being analysed.

Tortuosity parameter was determined only for three out of 12 samples tested from G-1 borehole (tab. 4). Sample 10729 distinguishes in this set in which connections between the opposite walls are present in all directions for both subsamples. These connections present similar pore throat tortuosity in three directions, while average tortuosity value oscillates around of 1.4 for X direction and 1.5 for Y and Z directions. Good transport properties for this sample are provided by pores of VI class, which constitute over 80% of its whole pore space. They dominated with its volume pores over other classes, enabling good fluid transport in all directions. Another sample which deserves attention is sample 10726 for which one subsample (10726B) has connections in three directions, and the second only for two (X , Z). Good transport properties of this sample have been provided also by pores of VI class, which constituted approx. 70% in sample 10726A, and even more in 10726B subsample – 88% (fig. 20).

Significant fraction of VI class pores, present in pore space of the sample, is a condition necessary for good saturation of rock pore space with media, but insufficient for the fluids migration in the rock. Lack of connections between pores limits the possibilities of fluids flow in a sample. Such conclusions result from the subsequent example concerning

Table 4. Results of pore throats geometric tortuosity measurement with micro-CT method

	Average tortuosity of pore throats τ_{avg} in direction:		
	X	Y	Z
10726A G-1 well	1.921	-	1.690
10726B	1.383	1.457	1.571
10729A	1.453	1.568	1.516
10729B	1.434	1.548	1.556
10730A	-	-	1.839
10735B O-3 well	-	-	1.610
10736A	1.642	1.402	1.647
10736B	-	2.299	1.851
10737A	1.638	1.268	1.291
10737B	1.568	1.296	1.353
10739A	2.474	-	2.809
10739B	-	-	1.746
10743A	1.299	1.329	1.330
10743B	1.351	1.460	1.339
10753B R region	2.857	-	2.283
10754B	-	-	2.218
10755A	1.172	-	1.172
10757B	1.888	-	1.902
10760A	-	-	1.520
10761A	1.845	1.596	2.252
10761B	2.056	1.785	1.949

sample 10730. Subsamples 10730A and 10730B in which the presence of VI class pores (33% and 20%, respectively) did not ensure connections between the opposite walls of subsample 10730B. Pores of class VI were better communicated in 10730A subsample, providing connections in Z axis direction, at tortuosity of pore throats averaging 1.84 (fig. 21).

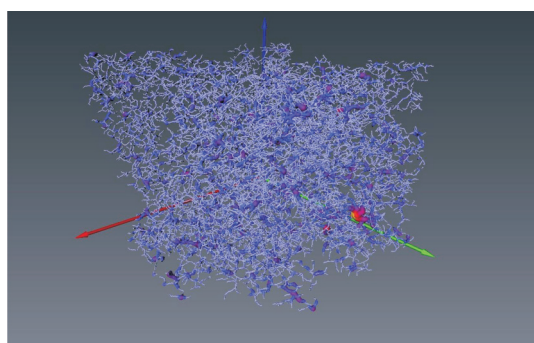


Fig. 20. Micro-CT image of all connected flow paths in 10726A sample

Average tortuosity of flow paths in direction X – 1.92, Z – 1.69

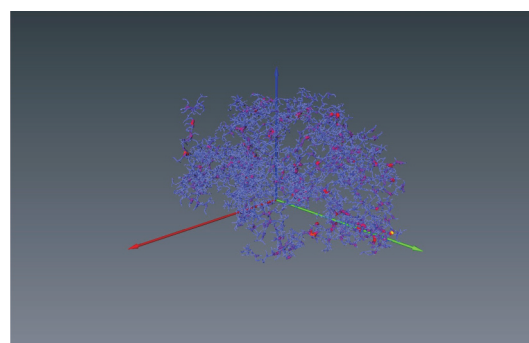


Fig. 21. Micro-CT image of all connected flow paths in 10730A sample

Average tortuosity of flow paths in direction Z – 1.84

(red colour – X axis, green colour – Y axis, blue colour – Z axis)

Examinations in O-3 borehole in scope of pore throats tortuosity were carried out on 12 samples, while determination of this parameter was done only for five of them (tab. 4). Samples 10743 and 10737 stand out in this sample set in which connections between opposite walls were present in all directions in both subsamples. Connections in 10743A and 10743B subsamples have low and almost equal value of pore throats tortuosity in three main directions: *X*, *Y*, *Z*, and average value of tortuosity oscillates around 1.3 value (tab. 4). Good transport properties of these samples were provided by pores of VI class, which constitutes 88% in 10743A subsample, and 84% in 10743B subsample within their whole pore space. They dominated pores of other classes with their volume, enabling good omnidirectional transport of fluid.

Prevalence of class VI pores in sample 10737 with very well developed pore structure is noted in both subsamples (85% of porosity in 10737A subsample, 77% of porosity in 10737B subsample), while *Y* and *Z* directions are privileged, considering the low value of tortuosity coefficient (1.27÷1.35). Connections of pore throats in subsample 10737B are slightly weaker than those in subsample 10737A. The values of tortuosity coefficient distribute similarly in both subsamples, which testifies to similar diversification of fluid flow path connections within pore space of the whole sample.

For sample 10736 where class VI pore volume makes up approx. 50% of total pore space volume, distribution of pores is non-uniform (fig. 22 & 23), but highly diversified routing of connection paths between opposing walls (1.4÷2.3) for *Y*, *Z* directions) ensured connections of pore throats in three directions for subsample 10736A and *Y*, *Z* directions for subsample 10736B. The entry to pore system in *X* direction for subsample 10736A is almost

twice as large as entries in *Y* and *Z* directions. The route of tunnels is highly diversified in all directions: the highest diversification is observed for *Z* direction, while the lowest for *X* direction. Average shape of channel in *Y* direction is closest to a straight line. The fraction of class VI pores in subsample 10736B is approx. 13% lower than in subsample 10736A; the pores did not provide connections in *X* direction. Connections of flow paths in the remaining directions have complex and diversified (especially in *Z* direction) shapes and medium surface of entry to pore system (tab. 4, fig. 22 & 23).

Much poorer results of pore throats geometric tortuosity measurement, evaluated with the use of micro-CT method, were obtained for subsamples 10739A and 10739B (tab. 4). Complexes of class VI pores ensured connections between opposite walls of subsample 10739A in *X* and *Z* directions. The connections have very complex shapes in both directions. The entry to the pore system in *Z* directions is fourfold smaller than for *X* direction, and connections, though more uniform, are more complex. In sample 10739B large pores provide connections in *Z* direction, at tortuosity of pore throats equal to 1.75. These connections feature complex shape and small surface of entry to the pore system.

The worst result of pore throats geometric tortuosity was obtained for sample 10735 from O-3 borehole. Although class VI pores dominated in pore space in both subsamples, their fraction was significantly lower than in the remaining samples. In subsample 10735B the connections of pore throats occurred in *Z* axis direction and they had shapes deviating from straight line (1.61) and the entry to pore network was very small. No connections of pore throats were documented in subsample 10735A.

Examinations concerning pore throats tortuosity for R

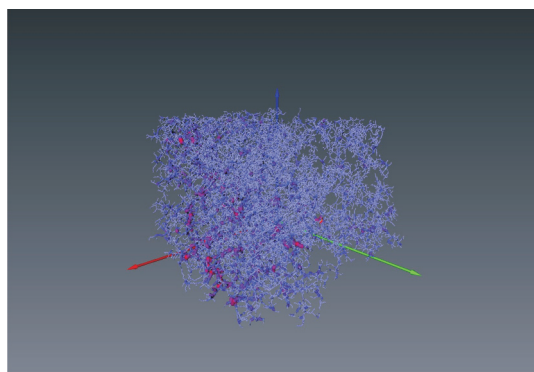


Fig. 22. Micro-CT image of all connected fluid flow paths in sample 10736A

Average tortuosity of flow paths in direction *X* – 1.64, *Y* – 1.40, *Z* – 1.65

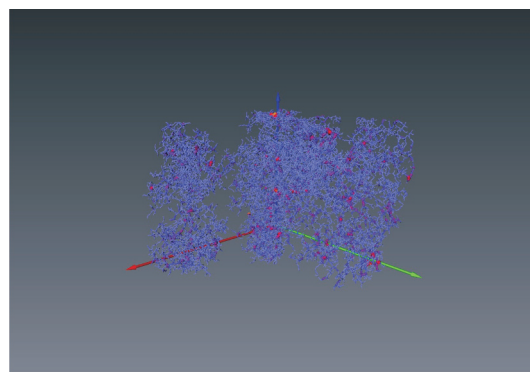


Fig. 23. Micro-CT image of all connected fluid flow paths in sample 10736B

Average tortuosity of flow paths in direction *Y* – 2.30, *Z* – 1.85

(red colour – *X* axis, green colour – *Y* axis, blue colour – *Z* axis)

region were carried out for 13 samples, while this parameter was determined only for six of them (tab. 4). Sample 10761 stands out in this collection in which connections between opposite walls are present in all directions for both subsamples, where pores belonging to volume class VI occupy 77% of the total volume of pores. The pore structure exhibits anisotropy of pore system, because in each of X , Y , Z directions of subsample 10761A the value of tortuosity coefficient is different: from $\tau_Y = 1.6$ up to $\tau_Z = 2.3$ (tab. 4). Tortuosity parameter determined for subsample 10761B has the lowest value $\tau_Y = 1.8$, and the highest value $\tau_X = 2.1$. One can note while comparing τ values for subsamples cut from single fragment of drill core that the increase in its value in Z direction for subsample 10761A does not correspond to the increase in the value for X direction in subsample 10761B. During the analysis of animations for pore structure of the whole sample and both subsamples, it is possible to note volume elements of spherical shape, having decidedly decreased porosity. The fragment of sample designated as 10753A, in micro-CT tortuosity examination revealed lack of connections

enabling media flow in any direction. It has been shown for sample 10753B that the possibility of medium communication between opposite walls in two directions: X and Z , do exists, at very high value of tortuosity coefficient (2.86 in X direction and 2.28 in Z direction).

The examinations have shown that pore distribution in both subsamples 10754A and 10754B is not uniform, but connections of pore throats occur only between walls perpendicular to the Z axis, and its tortuosity amounts to 2.22 (tab. 4).

Very good results in the aspect of fluids flow possibility were obtained for subsample 10755A in X and Z directions, which is related to the presence of the fracture which ensures connections of this subsample pore network between the walls perpendicular to the XZ plane. Coefficient $\tau = 1.17$ permits to conclude that the shape of connections is only slightly deviating from the straight line, for which $\tau = 1$. Values $\tau_X = \tau_Z$ enable to state high similarity degree of connection in both directions, X & Z . The entry to the pore system is small in both directions, which results from small width of the fracture.

Summary

Generally speaking all samples for which geometric tortuosity parameter has been determined, represented Aeolian dune sandstones of A2 facies, while only one sample originated from A2/A5 facies (10755A). Mean value of pore throat tortuosity in formations of the facies ranged from 1.17 up to 2.86.

Maximum tortuosity value for the longest flow paths, measured for all three directions ranged from 1.22 (sample 10755, X direction) up to 3.69 (sample 10761, Z direction), giving 2.17 mean value, while minimum tortuosity of the shortest measured flow paths belonged to the range from 1.10 to 2.19, with 1.39 average value.

The highest values of this parameter were observed for sandstone samples from R region, where the maximum measured tortuosity, also in three directions, changed within the range from 1.22 to 3.69. Tortuosity of the short-

est measured flow paths was found in samples originating from G-1 borehole and ranged from 1.20 to 1.77.

Summing up, it can be stated that based on microtomography data, samples of Aeolian dune sandstones of A2 facies, featuring the system of pretty large pores, have the best parameters. It is known from lithology description, that these are fine- and medium-grained sandstones, well and very well sorted, only sporadically having coarse sand fraction.

Pore space of rocks featuring the poorest parameters, represented by samples originating first of all from sandy P2 playa and marginal P1 playa facies, was dominated by micropores occurring in fine- and very fine-grained sandstones. They are secondary medium- and coarse-grained in marginal playa facies and they exhibit continuous or non-continuous lamination within sandy playa facies.

The article was sent to the Editorial Section on 18.02.2011. Accepted for printing on 28.04.2011.

Reviewer: prof. zw. dr hab. inż. Andrzej Kostecki

References

- [1] Dohnalik M., Zalewska J.: *Use of X-ray microtomography for solving of geological and geophysical issues*. INiG Works No. 157, monograph 2009, pp. 1–94.
- [2] Leśniak G. et al.: *Determination of processes leading to creation of anomalously low porosity and permeability in Aeolian sandstones in Poznań-Kalisz-Konin region and perspectives of "tight-gas" type reservoir discoveries in this zone*. Documentation of 395/SG order, 2009, Archive of INiG.
- [3] Zalewska et al.: *Evaluation of Upper Rotliegend sandstones pore space in G-R region, with the use of Nuclear Magnetic*

Resonance and X-ray microtomography methods. Documentation of 454/SW order, Archive of INiG.

- [4] Zalewska J., Dohnalik M.: *Determination of pore throats tortuosity with X-ray computed microtomography method*. Nafta-Gaz No. 12, pp. 953–958, 2009.

- [5] Zalewska J., Dohnalik M.: *Visualization and analysis of Rotliegend sandstones pore space with X-ray computed microtomography (micro-CT) method*. INiG Works No. 161, pp. 1–83, monograph 2009.



MSc Eng. Jadwiga ZALEWSKA – geologist, Academy of Mining and Metallurgy alumna. Head of Well Log Geophysics Department in Oil and Gas Institute – Krakow. Accomplishes research and development works in scope of laboratory measurements of drilling cores and muds for quantitative interpretation of well logs. Author of 132 published works.



MSc Jan KACZMARCZYK – Jagiellonian University Faculty of Chemistry graduate with specialization in catalysis and solid state surface chemistry. He was working in Oil and Gas Institute Well Logging Department. He conducted research on X-ray computed microtomography, image processing and fluid flow simulation.

ZAKŁAD GEOFIZYKI WIERTNICZEJ

- trójwymiarowa wizualizacja i analiza wewnętrznej struktury przestrzeni porowej skał metodą mikrotomografii rentgenowskiej (micro-CT);
- określanie rozkładu nasycenia wodą przestrzeni porowej próbek skał i kamienia cementowego metodą magnetycznego rezonansu jądrowego (NMR);
- oznaczanie jakościowego i ilościowego składu mineralnego skał oraz wydzielonej frakcji ilastej na podstawie analizy rentgenowskiej;
- wyznaczanie zawartości naturalnych pierwiastków promieniotwórczych: uranu, toru i potasu w skałach, płuczkach wiertniczych i materiałach budowlanych;
- ocena elektrycznych parametrów skał (wskaźnika struktury porowej i zwilżalności);
- określanie zależności elektrycznej oporności właściwej płuczek wiertniczych od temperatury;
- ocena prędkości propagacji fal ultradźwiękowych w skałach, kamieniach cementowych i płuczkach wiertniczych;
- interpretacja profilowań geofizycznych w zakresie oceny stanu zacementowania rur okładzinowych w otworach.



Kierownik: mgr inż. Jadwiga Zalewska

Adres: ul. Bagrowa 1, 30-733 Kraków

Telefon: 12 653-25-12 w. 132 lub 165

Faks: 12 650-67-70, 12 653-16-65

E-mail: jadwiga.zalewska@inig.pl